Rotating-wave-plate Stokes polarimeter for differential group delay measurements of polarization-mode dispersion

Paul A. Williams

We present a description and detailed uncertainty analysis of a polarization-mode dispersion (PMD) measurement system that uses the Jones matrix eigenanalysis measurement technique based on a rotating-wave-plate Stokes polarimeter. The uncertainty of the system is 3.2 fs (~95% confidence interval) and is due primarily to PMD in the fiber leads of the measurement system.

OCIS codes: 060.2270, 060.2300.

1. Introduction

We have assembled and tested a Jones matrix eigenanalysis (JME) measurement system for polarization-mode dispersion (PMD) measurements based on a rotating-wave-plate technique. This technique was used as the primary technique for calibrating a National Institute of Standards and Technology (NIST) Standard Reference Material (SRM 2518) for the generation of mode-coupled PMD.[1] Here, we calculate the uncertainty of the measurements.

2. Description of Apparatus

Our JME system is shown schematically in Fig. 1. Light from a tunable laser diode is coupled into a single-mode fiber and goes through a polarization controller and then through the specimen. The polarization state of the exiting light is measured with a Stokes polarimeter. The unusual aspect of our system, which differentiates it from other JME systems,[2–4] is that the Stokes polarimeter is based on a rotating-wave-plate design that uses a single detector (as opposed to four in other designs). Our design was chosen to minimize the possible errors in multiple-detector systems such as the gain mismatch that results from temperature gradients. Although multiple-detector implementations can calibrate out static gain mismatches between detectors and periodically recalibrate to minimize the effects of transitory gain mismatch due to thermal gradients, the single-detector design is simpler in that it does not require these calibrations. A personal computer is used to control the system and to analyze the intensity measurements.

The tunable laser has a range of 1480–1570 nm with a linewidth of less than 100 kHz. The free-space polarization controller consists of $\lambda/4$ and $\lambda/2$ wave plates, followed by a polarizer. The wave plates are used to manipulate the polarization state between the laser and the polarizer in order to optimize the power throughput. The polarizer P_1 has an extinction ratio of >40 dB from 1470 to 1570 nm. The orientations of the wave plates and the polarizer are computer controllable (the polarizer's orientational resolution is 0.18°).

The Stokes polarimeter consists of a graded-index lens that launches the light from the fiber onto a $\lambda/4$ waveplate (true zero-order polymer) spinning at 1450 rpm (~24 Hz). The light is then incident upon a Glan–Thompson analyzer P_2 whose extinction axis orientation is defined as horizontal. Exiting the analyzer, the light is incident on a lens and focused on an InGaAs photodiode. The output of the photodiode is read by a lock-in amplifier and a digital voltmeter (DVM). Measuring the dc, $2f$, and $4f$ components of this signal allows the calculation of the Stokes vector of the light (see Appendix A for details of the analysis).

The PMD of the test device is measured according to the technique of Heffner.[2] For a given test specimen, the Stokes vector of the transmitted light is measured at a particular wavelength for three dif-

P. A. Williams (paul.williams@nist.gov) is with the Optoelectronics Division, National Institute of Standards and Technology, MS 815.02, 325 Broadway, Boulder, Colorado 80303-3328.

Received 20 April 1999; revised manuscript received 12 July 1999.

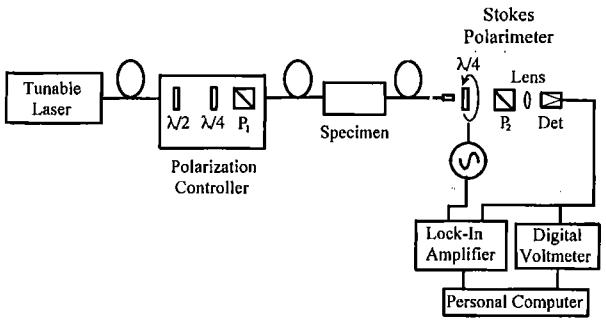

Fig. 1. Schematic of the rotating-wave-plate Stokes polarimeter for measuring DGD.

ferent launch polarization states (in our case, we use P_1 to generate three linear states at $\varphi + 0°$, $\varphi + 45°$, and $\varphi + 90°$ where φ is an arbitrary reference angle). From these three measured Stokes vectors, the Jones transfer matrix of the test specimen (including the fiber leads) is calculated at the test wavelength. Then, the wavelength is changed and the process repeated giving a second Jones matrix at the new wavelength. Again following Heffner, we calculate the differential group delay (DGD; or $\Delta\tau_g$) as

$$\Delta\tau_g = \left|\frac{\arg(\rho_1/\rho_2)}{\Delta\omega}\right|, \tag{1}$$

where ρ_1 and ρ_2 are the eigenvalues of the matrix product

$$T(\omega + \Delta\omega)T^{-1}(\omega), \tag{2}$$

formed from the Jones transfer matrices $T(\omega)$ and $T(\omega + \Delta\omega)$ of the test device measured at the two optical frequencies ω and $\omega + \Delta\omega$.

Here a couple of clarifying notes are appropriate. A DGD measurement requires measurement of the Jones matrix of the test specimen at two different optical frequencies. We usually refer to this difference in terms of wavelength as the step size. If the Jones matrices were measured at λ_1 and λ_2, then the calculated DGD would be reported as the DGD at the average of those two wavelengths. For example, if a scan of DGD versus wavelength involved measuring the Jones matrices at 1500, 1502, 1504, and 1506 nm (a 2-nm step size), then it would yield DGD values at 1501, 1503, and 1505 nm. For clarity, we use the term DGD to refer to the instantaneous group delay between the two principal states of polarization at a given wavelength. The term PMD is used to refer to the mean of multiple DGD measurements over a given wavelength range.

3. Uncertainty Analysis

The purpose of developing this JME measurement system was to provide accurate measurements of a NIST SRM for characterizing mode-coupled PMD.[1] The SRM is a stack of ~35 quartz wave plates cemented together with random angular orientations and pigtailed with single-mode fiber. Uncertainties in the assembly of this device prevented us from calculating its theoretical PMD; therefore the calibration of this device depends solely on the calibration of the JME system used to do the measurement.

We estimated the measurement system's type A (statistical) (Ref. 5) uncertainties from the standard deviation of multiple measurements. We also compared this result with the quadrature sum of estimated type A error sources.

Type B (nonstatistical) (Ref. 5) uncertainties, however, cannot be directly measured with self-consistency arguments (standard deviation, etc.). To identify them, we used two approaches. First, we tested the system by measuring a single pigtailed quartz plate (non-mode-coupled) with a known PMD. Second, we estimated the systematic uncertainties from the known inaccuracies of the experimental equipment.

The algorithm that derives PMD from the measured intensities is a complicated expression that does not lend itself to error analysis through simple propagation of errors. The best way to estimate PMD measurement uncertainty is through computer simulation. We wrote a program to generate the wavelength-dependent Jones matrices that represent a non-mode-coupled PMD element measured in the presence of equipment inaccuracies (polarizer misalignment, improper wave-plate retardance, etc.). These Jones matrices were fed into the same algorithms used by our JME system to calculate the measured DGD, and then this value was compared with the true theoretical value. The discrepancy is the error due to the equipment inaccuracies. This simulated experiment was repeated multiple times with various fiber pigtail orientations and different theoretical DGD values. The difference between these simulated DGD values (measured and true) gives an expected uncertainty due to equipment inaccuracies. Our simulations were run with DGD values uniformly distributed from 0 to 1 ps—the expected measurement range of our JME system for measuring the SRM artifacts.

In summarizing the uncertainties due to equipment inaccuracies, we found that most resulting measurement errors are random and that the significant systematic ones are systematic only for fixed measurement conditions. That is, if multiple measurements are made with the input state of polarization varied between measurement runs, all significant error sources will be random with a mean error of zero. We accomplished this by changing the launch polarizer offset (φ as mentioned above) before each DGD-versus-wavelength run. We also varied the launch polarization state by changing the orientation of the fiber leads connecting the specimen. Six possible sources of random error due to equipment inaccuracies were identified and are described below.

A. Random Uncertainties

1. Polarizer Misalignment

We measured the Jones matrix of the test device by launching three states of polarization with relative orientations of 0°, 45°, and 90°. Alignment errors of the polarizers cause negligible uncertainty in the measured DGD. As stated before, the 0°, 45°, and 90° angles are only relative orientations with respect to some arbitrary alignment. That means polarizer orientations of 10°, 55°, and 100° would give identical DGD values. It is only the relative offset between polarizer orientations that might cause trouble (0°, 46°, and 90° for example). We found from simulation that polarizer misalignments as large as ±2° give worst-case DGD errors less than $\pm 6 \times 10^{-4}$ fs. Since our expected alignment errors are on the order of 0.18°, polarizer misalignment is a negligible error source.

2. Lock-in Amplifier Phase Errors

Appendix A shows that the phase setting of the lock-in amplifier can be important. The signal distribution between the sine and the cosine components at $4f$ is determined by the phase setting of the lock-in amplifier. Phase errors at $4f$ cause leakage between S_1 and S_2 (horizontal and 45° linear states). This corresponds to a rotation of the defined Poincaré sphere about its polar axis. This leakage has no effect on DGD measurements, where the important parameter is the relative travel of the polarization state on the Poincaré sphere as a function of wavelength. However, incorrectly identifying S_1 and S_2 (C and D in Appendix A) does affect our measurement of degree of polarization (DOP). DOP is calculated as

$$\mathrm{DOP} = \frac{S_0 - (S_1^2 + S_2^2 + S_3^2)^{1/2}}{S_0}. \tag{3}$$

Since C and D are not used symmetrically in the Stokes parameter definitions of Eqs. (A6), phase errors at $4f$ cause us to misreport the DOP. This is important because we use DOP measurements to ensure that the system is well behaved during the measurement (we know that the DOP should be close to 1.0 and be a constant independent of measurement parameters). We easily set the $4f$ phase by launching a linear polarization state into the Stokes polarimeter (a bulk polarizer is placed immediately in front of the rotating wave plate at 90° with respect to the analyzer P_1 in Fig. 1). This vertical linear state has only a negative C component and no D component. We set the phase at $4f$ on the lock-in accordingly.

However, the phase setting at $2f$ directly affects the measured DGD, but fortunately by a small amount and in a random way. Since there is no $2f$ cosine term in Eqs. (A2)–(A5), errors in setting the phase at $2f$ reduce the amplitude of B. This distorts the Poincaré sphere by flattening it at the poles and can result in a second-order error in measurement of arc length on the sphere. We set the phase at $2f$ by launching a nearly circular state into the Stokes polarimeter and then adjusting the phase to optimize the amplitude of the B component. Our repeatability in setting phase is always less than 1°. So, we simulated the error in PMD measurements resulting from 1° phase errors on both $2f$ and $4f$ measurements and found the standard deviation to be 0.06 fs (for $\Delta\omega$ step sizes—see Eq. (2)—corresponding to 3 nm). Thus phase errors represent a negligible contribution to the measurement uncertainty.

3. Stokes Polarimeter

The primary source of errors in the measurement of the Stokes vector comes from imperfections in the quarter-wave retarder. The derivation of Appendix A assumes the retarder to be exactly quarter wave. If it is not, the result will be errors in the measured Stokes parameters. These errors are correctable if the true retardance of the wave plate is known. For a non-quarter-wave retarder, the true Stokes parameters are given by

$$\begin{aligned} S_0 &= A - C/\tan^2(\delta/2), \\ S_1 &= 2C/2\,\sin^2(\delta/2), \\ S_2 &= 2D/2\,\sin^2(\delta/2), \\ S_3 &= B/\sin(\delta), \end{aligned} \tag{4}$$

where δ is the true retardance of the nominally quarter-wave plate. These equations reduce to Eqs. (A6) when $\delta = 90°$. So, if the actual retardance of the quarter-wave plate is known, the true Stokes parameters can still be obtained. A problem occurs when there are unknown retardance variations in the quarter-wave plate.

The retardance of the wave plate is specified within 1.2° (manufacturer's specification of spatial uniformity). Computer simulations show that a 1.2° retardance error yields random measurement errors with a standard deviation of 8 fs. Other errors in retardance can result from a tilt between the wave plate and the incident beam and the wavelength dependence of the retardance. We measured the wavelength dependence of the quarter wave-plate retardance using the NIST rotating-polarizer polarimeter.[6] This wavelength dependence is used with Eqs. (4) for automatic correction of the wavelength-dependent retardance errors during the measurement.

Another potential source of uncertainty comes when the wave plate is tilted off axis. Wave-plate tilt takes two forms: Wobble is tilt of the wave plate in its mount with respect to the rotation axis, and axis tilt is tilt of the mount (rotation axis) with respect to the beam (Fig. 2). Pure wobble causes the light to enter the wave plate at nonnormal incidence, but with a constant angle of incidence with respect to the fast and the slow axes of the plate during rotation. This results in a systematic bias to the effective retardance of the wave plate. On our setup, we measured the wobble to be less than 0.4°. This translates to an internal (to the wave plate) incidence

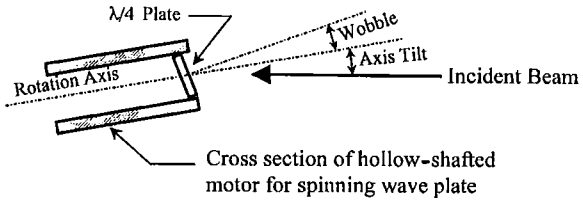

Fig. 2. Two possible types of wave-plate angular misalignment.

angle of 0.26°. This nonnormal incidence causes a systematic error in the wave-plate retardance of ±0.001°.[7] This is orders of magnitude below the uncertainty owing to wave-plate uniformity and is considered negligible. The effects of axis tilt are more difficult to quantify. The source of errors is still the same as with wobble—nonnormal incidence alters the effective retardance of the wave plate. However, as the plate rotates, the effective retardance changes, depending on whether the tilt is toward the fast or the slow axis (or somewhere between). We did not derive a closed-form expression to quantify this error, which depends on the DGD of the device being measured. Instead, we used computer simulation to predict the possible range of errors resulting from axis tilt. We measured the axis tilt to be <0.4° (external angle). Our simulation used a conservative estimate of 1° axis tilt, which gave a random error with a worst-case value of <0.03 fs. This represents a negligible error source.

4. Laser Wavelength

A significant source of uncertainty in the experiment can be attributed to uncertainty in laser wavelength. Using a wavemeter, we calibrated the wavelength error of the tunable laser (agreement between the target wavelength and the actual wavelength). Since we did not have a wavemeter available for real-time monitoring of the actual laser wavelength, we treated the wavelength uncertainty as an error source. In the measurement of DGD, a critical parameter is the wavelength difference $\Delta\lambda$ between adjacent measurement points. This is because the instantaneous DGD is given as $|dS/d\omega|$, the change in Stokes vector for a given change in optical frequency. An error in $\Delta\lambda$ therefore produces a proportional error in DGD. This error increases as the wavelength step size decreases. Our tunable laser exhibited a wavelength uncertainty of ±0.008 nm (one standard deviation). At, say, 8-nm step sizes, this represents only a 0.1% error, but at 0.8-nm step sizes, it becomes a 1% error. Fortunately, this error can be reduced by averaging of data (or by real-time monitoring of the laser wavelength with a wavemeter).

Computer simulation supports these statements. We ran simulations using worst-case wavelength errors of three times the observed ±0.008-nm standard deviation. For wavelength steps of 1 nm, random PMD errors with standard deviation σ = 12 fs occurred, 2-nm step sizes yielded σ = 5.7 fs, and 3-nm steps gave σ = 3.6 fs, for a nominal DGD of 0.5 ps.

Table 1. Estimated Random Uncertainties

Error Source	Standard Uncertainty, fs
Wavelength uncertainty (3-nm step size)	3.6
Multiple reflections (0.2% per surface)	3.6
Retardance error in λ/4 plate	8
Combined Standard Uncertainty	9.5

5. Multiple Reflections

One error that could occur independent of deficiencies in the measurement apparatus comes from multiple reflections. If two reflections somewhere in the test system occur with one on each side of the test specimen, then the effect will be a cavity with the test device inside. This means that the measured PMD includes coherently added PMD contributions from the multiple paths of the device. This type of phenomenon has been discussed in depth with regard to measurements of optical retardation.[8] In the case of PMD, the critical parameters are the same. The higher the quality factor Q of the cavity created by the reflections, the larger the distortion of the measured PMD. However, the saving fact is that the multiple delays with each reflection add coherently and so are very sensitive to wavelength and cavity length. Thus in PMD measurements, the effects of multiple reflections may be averaged away by multiple measurements either at slightly different temperatures (fractions of 1 °C should be enough) or at wavelengths that are different by fractions of 1 nm. Computer simulation showed that a cavity with intensity reflections of 0.2% (−27 dB) at each end and a true DGD of 0.5 ps generates a random DGD measurement error with a standard deviation of 3.6 fs.

6. Polarization Extinction Ratio

The two polarizers used in the system have extinction ratios ≥40 dB. However, the extinction ratio of the polarizers is not critical since the JME measurement calculates the DGD only from the portion of light that is completely polarized. A poor extinction ratio of P_1 would reduce the degree of polarization through the test device, but only the polarized part of the light is used in the DGD measurement. Poor extinction by P_2 would underreport the DOP of the light going through the test device. But, low extinction ratios in either P_1 or P_2 do not directly affect the PMD accuracy. The only reason for high extinction ratios on the polarizers is to optimize the optical throughput for purposes of noise reduction.

7. Summary of Random Uncertainties

Table 1 lists the theoretical sources of random uncertainty (one standard deviation) and their combined standard uncertainty (quadrature addition) total of 9.5 fs. We directly measured the standard deviation of DGD measurements with a pigtailed quartz plate (0.4464 ps). We made 50 scans over the range 1480–1569 nm, giving a total of 1008 data points.

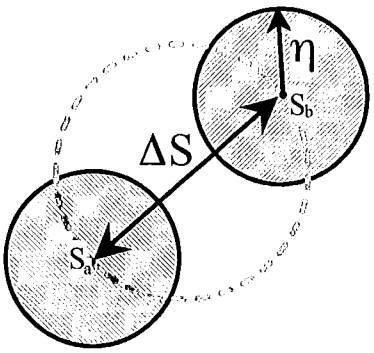

Fig. 3. Schematic illustration that the distance ΔS between two Stokes vectors ($\mathbf{S_a}$ and $\mathbf{S_b}$) is systematically biased by the presence of random Stokes noise (of amplitude η).

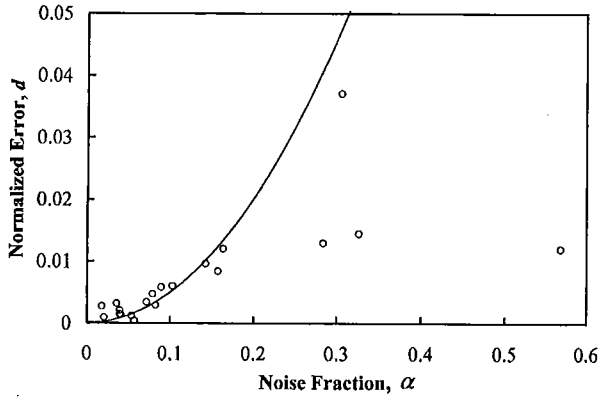

Fig. 4. Normalized systematic error $d(\alpha)$ versus noise fraction α. Solid curve is theoretical prediction from Eq. (5), and circles are data points from two different quartz plates sampled at different wavelength step sizes.

The measured sample standard deviation was 5.2 fs, and the standard deviation of the mean was 0.20 fs. This 5.2-fs experimental standard deviation is well within our 9.5-fs estimate.

B. Systematic Uncertainties

1. *Systematic Errors from Random Noise*

It is possible for a random-noise source to add a systematic bias to PMD measurements. This comes from the fact that DGD is a scalar quantity resulting from a vector measurement. The JME measurement of DGD is equivalent to measurement of the change in the output Stokes vector in response to a change in the optical frequency of the source $|\Delta S/\Delta\omega|$. Figure 3 shows the Stokes vectors ($\mathbf{S_a}$ and $\mathbf{S_b}$) measured at λ_a and λ_b, respectively. If the measured Stokes vectors are subject to some noise η, they will randomly describe a set of points within a circle of radius η whose center is the location of the noise-free Stokes vector. When measuring arc length on the sphere, the average of multiple JME system measurements really averages the distance between points randomly located within circle a and points randomly located within circle b. This operation does not average to the distance between the circles' centers ($\Delta S = |\mathbf{S_a} - \mathbf{S_b}|$) but rather to something greater than that. This seems counterintuitive, but consider the case in which ΔS approaches 0; measuring ΔS then amounts to the average distance between two points randomly chosen within a circle of radius η. Clearly, this average distance is greater than 0; thus we have a positive systematic bias. This normalized error in measuring DGD in the presence of noise can be approximated as

$$d(\alpha) = \frac{\int_0^{2\pi}\int_0^{2\pi} [(1 + \alpha\cos\theta - \alpha\cos\varphi)^2 + (1 + \alpha\cos\theta - \alpha\cos\varphi)^2]^{1/2}\, d\theta d\varphi}{\int_0^{2\pi}\int_0^{2\pi} d\theta d\varphi}, \tag{5}$$

where the noise fraction $\alpha = \eta/\Delta S$. This normalized theoretical bias is plotted as a function of α in Fig. 4 (solid curve). The data points are experimental data from measurements of two quartz plates of PMD at 0.218 and 0.4464 ps. We varied α experimentally by sampling with various wavelength step sizes. As Fig. 4 shows, the systematic bias in the measurements agrees well with theory for small values of α. To determine α for the experimental data, we knew the target value of ΔS, and we used η as the free parameter. The points in Fig. 4 are scaled with $\eta = 0.015$. These values agree fairly well with the estimated η values for our apparatus. We can estimate η as $\eta_S + \eta_\lambda$, where η_S is a direct measurement of the random noise on the Stokes vector and η_λ is the estimated noise due to the random wavelength variations. The expression $\eta_S + \eta_\lambda$ yields a value between 0.006 and 0.009. This discrepancy between predicted and fitted values of η implies that there are still other random-noise sources that we have not accounted for.

This possible systematic error in measurements must be considered when the PMD-induced Stokes vector change is small with respect to the absolute noise on the measurement. In our calibration measurements, this was not a factor since our measurements were carried out with step sizes between 2.7 and 8 nm ($\alpha < 0.009$), which yields negligible systematic uncertainties. However, as can be seen from Fig. 4, the experimental data level off without reaching zero at the smallest values of α. This effect, which likely comes from some other source of error

Table 2. Summary of Measurement Uncertainty for JME Measurement System

Uncertainty Source	Method	Standard Uncertainty, fs
Experimental random errors	Measured standard deviation of the mean of repeated independent measurements	0.20
Systematic bias due to random noise	From random-noise estimates	1.0
Uncertainty of quartz artifact calibration	Theoretical calculation	1.2
Combined standard uncertainty	$u_c = [\Sigma u_i^2]^{1/2}$	1.6
Expanded uncertainty	$U = 2u_c$	3.2

than was considered here, can be taken into account by addition of a conservative +0.2% (~1 fs for our ~0.5-ps device) contribution to the uncertainty. Although these systematic errors are practically negligible for the current measurements, this bias mechanism must be kept in mind because it limits the minimum wavelength step that may be used in measurements. For example, given the noise of this system, a <0.25% systematic uncertainty requirement means that a 0.1-ps device must be measured with a step greater than 0.5 nm and that a 1-ps device requires steps greater than 0.2 nm.

2. *Comparison to Artifact*

To calibrate our JME measurement system and identify systematic errors, we measured our well-characterized pigtailed quartz plate (Appendix B). As described above, 1008 measurements were made over the wavelength range 1480–1569 nm with step sizes between 2.7 and 8 nm. The average of the measurements was 0.4465 ps with a sample standard deviation of 5.2 fs. The difference between our measurement of the PMD of the quartz plate and the 0.4464-ps theoretical value is 0.1 fs, well within the 1.2 fs uncertainty of the quartz plate's theoretical PMD.

3. *Quality of Data*

Since much of the uncertainty analysis of this system relies on assumptions about the uncertainties of the measurement equipment, it is useful to have an independent means of judging if the data has been taken under the assumed conditions. The measured DOP was used for this purpose. Particular error sources such as wave-plate retardance errors, lock-in phase errors, Stokes noise, and dc measurement errors cause the measured DOP to fluctuate around its true value. For these error sources, the size of DOP fluctuations can be an indication of the magnitude of the measurement uncertainty. We have found through simulation that for uncertainties within ranges that support our error-analysis assumptions, the DOP varies by as much as ±5% or so. So, to be conservative, we measure DOP simultaneously with DGD and use only those DGD values that fluctuate about the mean by less than 3%. Experimentally, we find a mean DOP of 0.97 for measurements with our system. So we throw out DGD values that have an associated DOP outside of the range $0.94 < \text{DOP} < 1.0$. As a test, we compared mean DGD measurements made on the pigtailed quartz-plate artifact with and without this DOP criteria and found only a 0.01-fs difference. This supports our assumptions regarding equipment uncertainties and implies that this DOP criteria was not necessary.

4. Conclusions

Table 2 lists the significant uncertainties (in femtoseconds) that we have calculated for our measurement system for measurements on a ~0.5-ps device. Adding the three uncertainties in quadrature and multiplying by a coverage factor of 2 gives an expanded uncertainty of 3.2 fs. For comparison, we are aware of one other published uncertainty analysis for a polarization-state analyzer that uses the Stokes vector arc analysis technique for DGD measurement.[4]

Appendix A: Operation of Stokes Polarimeter

The polarization state of the light is determined with a rotating-wave-plate Stokes polarimeter.[9] As Fig. 1 shows, the Stokes polarimeter is simply a spinning quarter-wave plate in front of a fixed polarizer, followed by a detector. Using a phase-sensitive lock-in amplifier and a dc voltmeter allows the measurement of the dc, $2f$, and $4f$ (both in-phase and quadrature components). The four Stokes parameters can be found from these components. At the detector, the intensity as a function of wave-plate orientation θ and the Stokes parameters of the incident light is[9]

$$I(\theta) = \frac{1}{2}(S_0 + S_1 \cos^2 2\theta + S_2 \sin 2\theta \cos 2\theta + S_3 \sin 2\theta), \quad \text{(A1)}$$

where S_0 is the first Stokes parameter of the incident light, and so on. One can find the Stokes parameters by Fourier analyzing the transmitted intensity. The dc signal is measured, with a DVM, as

$$A = \frac{1}{\pi}\int_0^{2\pi} I(\theta)\mathrm{d}\theta, \quad \text{(A2)}$$

where $I(\theta)$ is the detected intensity when the wave plate has orientation θ. The $2f$ component is measured with the lock-in amplifier to give

$$B = \frac{2}{\pi}\int_0^{2\pi} I(\theta)\sin(2\theta)\mathrm{d}\theta. \quad \text{(A3)}$$

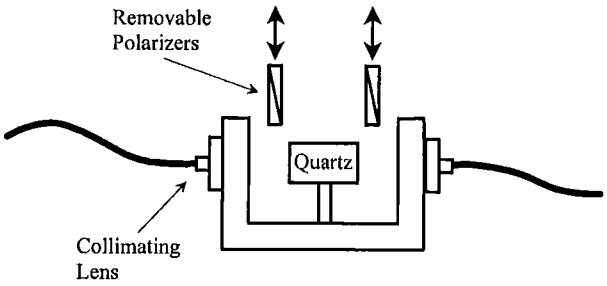

Fig. 5. Diagram of non-mode-coupled PMD test artifact. With removable polarizers that can be inserted to make a wavelength-scanning measurement independent of lead PMD.

The $4f$ components are

$$C = \frac{2}{\pi}\int_0^{2\pi} I(\theta)\cos(4\theta)\mathrm{d}\theta, \tag{A4}$$

$$D = \frac{2}{\pi}\int_0^{2\pi} I(\theta)\sin(4\theta)\mathrm{d}\theta. \tag{A5}$$

The Stokes parameters are found by combination of the measured values A, B, C, and D to give

$$\begin{aligned} S_0 &= A - C, \\ S_1 &= 2C, \\ S_2 &= 2D, \\ S_3 &= B. \end{aligned} \tag{A6}$$

The resulting Stokes vector is then used along with the two other Stokes vectors measured for different orientations of the input polarizer to calculate the Jones transfer matrix of the device under test. This procedure is also included in Heffner's letter.[2]

The advantage of the rotating-wave-plate method of measuring the Stokes parameters is that all four parameters are measured with the same detector. This eliminates the errors that can result from a four-detector system with mismatched gains.

The dc level A is measured with a DVM as opposed to the lock-in amplifier used for B, C, and D. This means that errors in the absolute calibration between the DVM and the lock-in could be important. However, the dc level is used only in the calculation of DOP and has no effect on measured DGD.

Appendix B: Quartz-Plate Reference Device

To assess the accuracy of the measurement system, we measured an artifact of known PMD and compared our measured result with the known value. We did this by assembling a non-mode-coupled artifact from a single quartz plate pigtailed with single-mode fiber (Fig. 5). We measured the thickness and wedge of the quartz plate accurately and combined that information with group birefringence data to calculate the expected DGD for propagation through the quartz plate. The uncertainty of the DGD of the plate comes from uncertainties of the thickness and index measurements, birefringence in the fiber pigtails, and multiple reflections off the endfaces of the quartz.

We measured the thickness of the quartz plate with a coordinate-measurement machine. The plate's thickness was 14.243 ± 0.002 mm (±0.014%), measured at 20.2 ± 0.2 °C. Another factor in the uncertainty is the effective thickness of the quartz plate. Although we accurately know the thickness of the plate, if the probe light enters the plate at a nonnormal incidence, the optical path length will be different. We measured the angle of incidence φ for He–Ne light at 632.8 nm to be 0.31°, which translates to an internal angle of 0.21°. Assuming this angle to be the same as for light at the actual wavelength of use (~1550 nm), we calculate the tilt-induced length error to be +0.0001 − 0 mm, or <0.0007%, again negligible in light of the absolute thickness uncertainty of ±0.014%.

We obtained the quartz birefringence in two different ways. First, comparison of the numbers from the literature[10–12] illustrates a discrepancy in the quoted values (>0.18%). So, as a second approach, we measured group birefringence ourselves. The quoted journals report phase birefringence as opposed to group birefringence. It is the group birefringence that determines the DGD. The relation between the two is[13]

$$\Delta n_g = \Delta n_p - \lambda \frac{\mathrm{d}(\Delta n_p)}{\mathrm{d}\lambda}. \tag{B1}$$

We made the group birefringence measurement by a wavelength scan of the quartz plate (Fig. 5). We inserted polarizers between the graded-index lenses of the fiber pigtails and the quartz plate to eliminate birefringence due to the leads. The transmitted intensity versus wavelength was recorded for the polarizers in a crossed orientation. The 90-nm scan range (centered at 1525 nm) yielded multiple nulls corresponding to the condition that the retardance $\Delta nL/\lambda$ of the quartz plate was an integer. For the conditions described, those integers were near 77, depending on the order of null. Therefore, as long as our estimate of $\Delta nL/\lambda$ was better than 0.5 parts in 77 (0.65%), we would be able to determine the order number of a given null unambiguously. Then, forcing $\Delta nL/\lambda$ to be equal to that integer gives a more accurate estimate of Δn. As stated, published values of Δn differed by 0.18%. Since this uncertainty is significantly less than the required 0.65% (as are the 0.014% thickness uncertainty and the 0.0005% wavelength uncertainty), we can identify the order of each fringe. For example, using a literature value $\Delta n_{\mathrm{lit}}(\lambda)$, for a particular null λ_{null}, $\Delta n_{\mathrm{lit}}(\lambda_{\mathrm{null}})L/\lambda_{\mathrm{null}} = 77.009$. Our accuracy is good enough to say that the true order of this null is 77 (not 76 or 78). We then correct for the least accurate parameter $\Delta n_{\mathrm{lit}}(\lambda)$ so that $\Delta n_{\mathrm{corr}}(\lambda_{\mathrm{null}})L/\lambda_{\mathrm{null}} = 77$ exactly. Doing so over the 90-nm wavelength range, we have improved the accuracy of our Δn estimate by an order of magnitude

so that it is limited by the length uncertainty of 0.014%.

The PMD of the quartz plate is $\Delta nL/c$ (where c is the speed of light), and we found it to be equal to 0.4467 ps for a 89-nm scan centered at 1524.5 nm. The uncertainty on this number is due to the uncertainty of L (0.014%) and Δn ($\pm$0.014%). Adding in quadrature gives $\pm$0.02% or 0.09 fs. The birefringence of the fiber leads themselves was measured (in the absence of the quartz plate) to be approximately 1.2 fs. This is not an exact estimate of the error due to lead birefringence since as the leads are repositioned, the PMD of the leads add to or subtract from the PMD of the device. Moving the leads between measurements averages the effect of lead birefringence, but not completely. Some birefringence is likely to be in the graded-index lenses themselves, and their orientation does not change when the leads are moved. We therefore estimate the uncertainty on the PMD of the artifact to be the quadrature sum of the 0.09-fs uncertainty of the quartz plate and the 1.2 fs of the leads, giving an overall 1.2-fs uncertainty dominated by lead birefringence. We obtain an approximately 95% confidence interval by using a coverage factor of 2. Therefore we estimate the PMD of the pigtailed quartz plate to be 0.4467 $\pm$ 0.0024 ps at 1524.5 nm and 20.2 °C.

Our JME measurements of the quartz plate's PMD were carried out at a temperature of 23.3 $\pm$ 0.1 °C. We therefore modify our estimate of the PMD to this temperature. The thermal expansion of quartz, $\alpha = 13.6 \times 10^{-6}$/°C (Ref. 14) couples with the temperature dependence of the birefringence to give a temperature dependence to PMD. The temperature dependence of the retardance of quartz at 1525 nm is assumed equal to a value measured at 1535.59 nm,[15]

$$\gamma = (1/\Delta nL)\mathrm{d}(\Delta nL)/\mathrm{d}T = -1.232 \times 10^{-4}/°\mathrm{C}.$$

Using γ, we estimate the PMD of the quartz plate to be 0.4464 $\pm$ 0.0024 ps at 23.3 °C and 1524.5 nm.

References and Notes

1. P. A. Williams, "Mode-coupled artifact standard for polarization-mode dispersion: design, assembly, and implementation," Appl. Opt. **38,** 6498–6507 (1999).
2. B. L. Heffner, "Automated measurement of polarization mode dispersion using Jones matrix eigenanalysis," IEEE Photon. Technol. Lett. **4,** 1066–1069 (1992).
3. See "Polarization-mode dispersion measurement for single-mode optical fibers by Jones matrix eigenanalysis," *Fiber Optic Test Procedure (FOTP) 122* Telecommunications Industry Association, 2500 Wilson Blvd., Suite 300, Arlington, VA 22201 USA.
4. D. J. Ives, "Calibration of a polarisation state analyser for polarisation mode dispersion measurements," in *Technical Digest of the Fourth Optical Fibre Measurement Conference* (Teddington, UK, 1997), pp. 213–216. The exact form of the Stokes polarimeter in this reference is unclear, however, a detailed error analysis is carried out.
5. The terms type A and type B uncertainties refer to the ISO and the NIST convention and denote uncertainties that are (A) evaluated by statistical means and (B) evaluated by nonstatistical means. For details, see B. N. Taylor and C. E. Kuyatt, eds., "Guidelines for evaluating and expressing the uncertainty of NIST measurement results," National Institute of Standards and Technology, TechNote 1297 (National Institute of Standards and Technology, Boulder, Colo., 1994).
6. P. A. Williams, A. H. Rose, and C. M. Wang, "Rotating-polarizer polarimeter for accurate retardance measurement," Appl. Opt. **36,** 6466–6472 (1997).
7. P. D. Hale and G. W. Day, "Stability of birefringent linear retarders (waveplates)," Appl. Opt. **27,** 5146–5153 (1988).
8. K. B. Rochford, A. H. Rose, P. A. Williams, C. M. Wang, I. G. Clarke, P. D. Hale, and G. W. Day, "Design and performance of a stable linear retarder," Appl. Opt. **36,** 6458–6465 (1997).
9. E. Collette, ed., *Polarized Light: Fundamentals and Applications* (Marcel Dekker Inc., New York, 1993), p. 103.
10. J. H. Shields and J. W. Ellis, "Dispersion of birefringence of quartz in the near infrared," J. Opt. Soc. Am. **46,** 263–265 (1956).
11. W. L. Wolfe and G. J. Zissis, eds., *The Infrared Handbook* (Environmental Research Institute of Michigan, Ann Arbor, 1985), pp. 7–57.
12. B. L. Heffner, "Attosecond-resolution measurement of polarization mode dispersion in short sections of optical fiber," Opt. Lett. **18,** 2102–2104 (1993).
13. J. D. Jackson, *Classical Electrodynamics* (Wiley, New York, 1975), p. 302.
14. D. E. Gray, ed., *American Institute of Physics Handbook* (McGraw-Hill, New York, 1972), pp. 4–138.
15. A. H. Rose and S. M. Etzel, National Institute of Standards and Technology, Boulder, Colo., 80303 (personal communication).